

Enhancing ORR Performance of Bimetallic PdAg Electrocatalysts by Designing Interactions between Pd and Ag

Luis E. Betancourt, Arnulfo Rojas-Pérez, Ivan Orozco, Anatoly I. Frenkel, Yuanyuan Li, Kotaro Sasaki, Sanjaya D. Senanayake, and Carlos R. Cabrera*

Cite This: *ACS Appl. Energy Mater.* 2020, 3, 2342–2349

Read Online

ACCESS |



Metrics & More



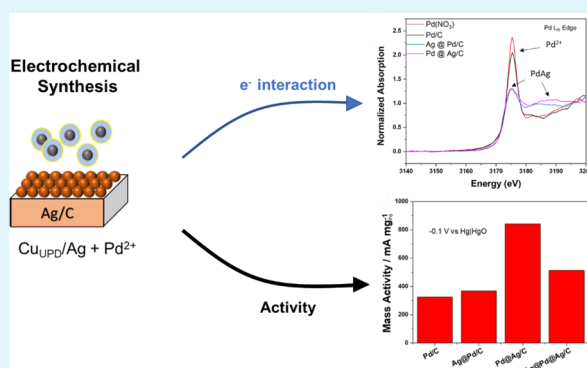
Article Recommendations



Supporting Information

ABSTRACT: Precise tuning of the electronic properties of Ag/C using under potentially deposited (UPD) Cu and subsequent galvanic displacement to deposit atomically dispersed loading of Pd resulted in a robust bimetallic alloy with significant activity for the oxygen reduction reaction in alkaline media. The specific design of the catalyst and atomic arrangement of Pd–Ag outperforms conventional Pd/C and Ag/C commercial catalysts. The ORR activity of Pd deposited onto Ag/C was determined on the basis of rotating disk electrode voltammetry studies, showing a 2-fold increase in Pd mass activities compared to results obtained using Pd/C. While scanning transmission electron microscopy (STEM) coupled with electron energy loss spectroscopy (EELS) probed the uniformity of the nanoparticles, the origin of the outstanding activity was traced to the structural properties of the Pd–Ag interface as shown by X-ray absorption spectroscopy (XAS), along with X-ray photoelectron spectroscopy (XPS). Segregation of metals with a suitable geometric arrangement of the Ag to Pd ratio at the interface resulted in an increased performance where the active sites were key steps of oxygen bond breaking.

KEYWORDS: electrocatalysis, oxygen reduction, Ag/Pd bimetallic nanoparticles, galvanic displacement, Cu UPD



INTRODUCTION

The oxygen reduction reaction (ORR) is an essential energy conversion process typically used for energy-storing devices such as batteries and fuel cells.¹ This is particularly true for fuel cell vehicles for which the potential growth of the market and the concern for abundant gas emissions urge the design of catalytic systems with improved activity. Efforts are geared toward decreasing the amount of Pt or finding a substitute with adequate ORR activity.^{2–4} A promising approach is to design new electrocatalysts having monolayer amounts of a noble metal on the surface of suitable metallic nanoparticles.^{5–7} For that reason, a catalyst support such as carbon is essential for the proper dispersal of metal nanoparticles by acting as a path of electrons, thus increasing electrical conductivity while simultaneously reducing metal loadings.⁸ Electrochemical approaches generally lead to higher control over particle and distribution size, creating stronger interactions between metal and substrate.⁹ Ag-based formulations have been found to have adequate oxygen reduction reaction (ORR) activity; however, the incorporated Pd yields additional benefits due to its unique catalytic features and distinct Ag–Pd interactions.¹⁰ Experimental¹¹ and computational studies suggest that an enhanced Ag–Pd interface can improve significantly the catalytic activity of these materials.^{7,12,13} In particular, the presence of Pd with Ag can lead to flexible control of the d band center via ligand

effects exerted between the host metal and subsurface metal atoms. According to computational studies, a volcano plot shows that, for ORR activity, Ag and Au bind weakly to oxygen, whereas other transition metals (e.g., Ni, Cu, Rh, Pd) bind strongly to both O₂ and hydroxyl species.¹² Therefore, a combination of Ag and Pd at a suitable geometric arrangement may give optimum binding of O for the ORR.¹⁴

The electrochemical oxygen reduction in alkaline media of Pd and Ag-based catalysts has been highlighted in recent review articles.^{15–17} However, the electrochemical oxygen reduction behavior of Ag-containing alloys still requires further insight. The high reactivity for ORR over the Pd–Ag alloy was recently described by the Stevenson group, where they produced stable bimetallic nanoalloys via coreduction of Ag and Pd carboxylic acid complex precursors at similar rates¹⁸ in the presence of stabilizing ligands.¹¹ In their study, Ag–Pd nanoalloys are shown to favor the oxygen reduction reaction at a Ag:Pd composition of 9:1. These alloys exhibited a suitable

Received: September 28, 2019

Accepted: February 18, 2020

Published: February 18, 2020



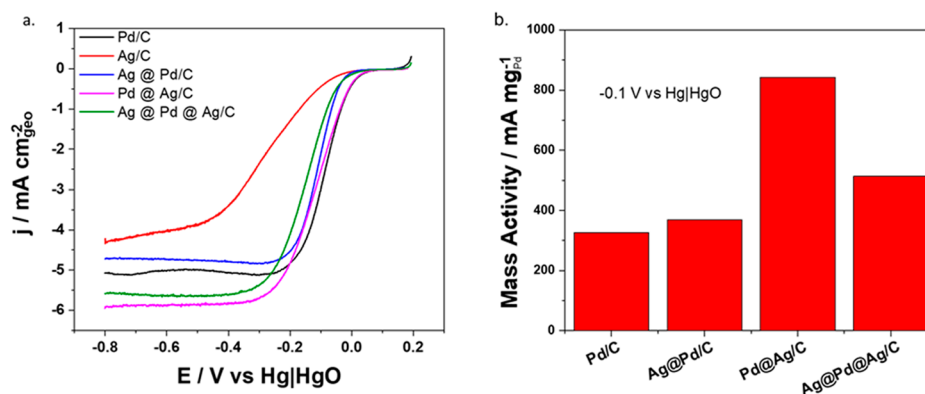


Figure 1. Electrochemical oxygen reduction reaction (ORR) activity comparison between Ag and Pd alloys and their pure constituents: (a) linear sweep voltammogram from a rotating disk electrode measurement at 1600 rpm in O₂-saturated 0.1 M KOH from 0.2 V to -0.8 V vs Hg|HgO at 10 mV/s and (b) bar plot representation of ORR activity at -0.1 V vs Hg|HgO normalized per Pd loading.

geometric arrangement allowing to work by an ensemble effect, where the Pd atoms can facilitate the binding of the initial oxygen and subsequently the Ag can help desorb the reaction products such as OH. In such a way, the full four-electron process takes place by combining the fast kinetics of Pd for the adsorption with rapid disproportionation on Ag for the desorption step. To the best of our knowledge, electrochemical routes, which provide an enrichment of Ag at a AgPd alloy, have not been previously reported.

Previous work by Lüsi et al. showed the use of galvanic displacement on an electron-beam-evaporated Cu used to prepare thin film Pd electrodes tested for the ORR reaction in alkaline media.¹⁹ This active arrangement gave a four-electron pathway similar to that of commercial Pd/C making Cu a suitable sacrificial agent to be galvanically displaced by Pd. For this work, Pd nanoparticles were systematically deposited onto a UPD layer of Cu adatoms onto Ag/C via galvanic displacement; in addition, Ag nanoparticles were deposited onto a UPD layer of Cu adatoms onto Pd/C.¹⁹ Characteristics of the preparation method, properties, and performance of the catalyst have been investigated in detail. The data suggest a correlation between the bimetallic interaction developed at the nanoscale and the observed high catalytic activity. For consistency purposes, both Pd deposited onto Ag/C (Pd@Ag/C) and Ag deposited onto Pd/C (Ag@Pd/C) were prepared in tandem.

These bimetallics were prepared using a high corrosion resistance cell made of a graphite plate, which acted as the working electrode, and a reducing potential was applied with respect to the Ag/AgCl reference electrode with a platinum flag used as the auxiliary electrode. Commercial 30% Pd/C (E-TEK, 10 wt %, 3.5 nm Pd particle size) and 40% Ag/C (Premetek, 40 wt %, 5.0 nm Ag particle size) were used as reference catalysts. The details on sample preparation and the electrochemical parameters used are given in the Supporting Information (Figure S1), along with the detailed description of electrochemical testing conditions and electron microscopy characterization methods.

EXPERIMENTAL SECTION

Synthesis of Bimetallics. An electrochemical cell with a high corrosion resistance made of graphite acted as a working electrode (14 cm diameter). A 2 g portion of commercially available carbon supported Pd nanoparticles was placed on the bottom of the cell. The Pd/C nanoparticle surface was electrochemically reduced by applying

a potential between the working electrode and a leak-less Ag|AgCl electrode with a platinum flag as the auxiliary electrode. Afterward, a concentrated CuSO₄ solution was added to adjust the concentration of Cu²⁺ in the cell to 50 mM. A constant potential (100 mV vs Ag|AgCl) was then applied to form UPD Cu adatoms on the Pd nanoparticle surfaces. The solution was stirred while the constant potential was applied, to disperse the Pd/C particles in the electrolyte, ensuring the formation of UPD Cu monolayers on the Pd surfaces. Cu UPD is carried out until the current reached a steady current value near zero. After Cu monolayers, a Ag⁺ solution of AgNO₃ in a 50 mM H₂SO₄ on a separate reservoir was injected slowly into the cell while it remained vigorously stirring to allow Ag⁺ ions to replace the Cu monolayer on Pd surfaces via galvanic displacement. The amount of metal salt precursor used was calculated for a monolayer amount of catalyst with respect to the host metal while taking into consideration the stoichiometry of the reaction with respect to Cu⁺. The same technique was used to deposit Pd onto Ag/C using a solution of PdCl₂ with Pd²⁺ as precursor afterward.

Characterization Techniques. Transmission electron microscopy (TEM), high annular dark field scanning electron microscopy (HAADF-STEM), and electron energy loss spectroscopy (EELS) for elemental mapping were conducted on a high resolution, analytical scanning/transmission electron microscope (S/TEM, FEI Talos F200X). Images were taken by operating at 200 keV at the Center for Functional Nanomaterials, BNL. XAS measurements were performed at the National Synchrotron Light Source-II (NSLS-II), Brookhaven National Laboratory (BNL) using Beamlines 8-ID and 8-BM. The measurements were carried out using the Pd L_{III}-edge (3173 keV), Pd K-edge (24 350 eV), and Ag K-edge (25 514 eV) in fluorescence mode and with a passivated implanter planar silicon (PIPS) detector. Data processing was performed using the IFEFFIT package.²⁰ A commercial SPECS AP-XPS chamber equipped with a PHOIBOS 150 EP MCD-9 analyzer at the Chemistry Division of BNL was used for XPS analysis. The C 1s (284.5 eV) feature was used for energy calibration.²¹ The catalyst in the form of a powder was pressed on an aluminum plate and then loaded into the XPS chamber. The mass weight % was determined by inductively coupled plasma-atomic emission spectroscopy (ICP-AES). The catalyst was electrochemically cycled from -0.8 to 0.2 V vs Hg|HgO at 20 mV/s for 10 cycles under Ar to clean the surface in 0.1 M KOH. Following this cleaning procedure, an extended cyclic voltammetry (CV) from -0.9 V to 0.9 V at 20 mV/s was performed to identify the oxidation/reduction peaks for both Ag and Pd. The electrolyte was then saturated with oxygen bubbling in the solution for 10 min. ORR activity measurements were taken by rotating the electrode at 1600 rpm, performing a linear sweep from 0.2 V to -0.8 V at 10 mV/s.

RESULTS

The polarization curves at 1600 rpm for the studied catalysts for the ORR reaction together with their pure Pd and Ag metal components are shown in Figure 1a. Quantitative ORR kinetic parameters obtained at 1600 rpm under ORR conditions can be observed in Table 1. The overall performance of the

Table 1. Quantitative ORR Kinetics Parameters Calculated for the ORR in 0.1M KOH

catalyst	normalized Pd mass activity (mA mg ⁻¹)	E_{onset} (mV)	$E_{1/2}$ (mV)	no. of electrons ^a
Ag/C		-59	-261	2.5
Pd/C	341	-12	-86	3.7
Ag@Pd/C	396	-6	-108	3.4
Pd@Ag/C	878	-37	-117	4.0
Ag@Pd@Ag/C	578	-50	-156	3.4

^aNumber of electrons were calculated applying the Koutechy–Levich equation.

samples was strongly influenced by the presence of Pd in the catalyst. Modifying Pd/C by incorporating Ag (blue curve in Figure 1a) decreases the diffusion limited current density (j_D) and shifts the ORR half wave potential ($E_{1/2}$) closer to Ag/C (red curve) thereby increasing its overpotential for the ORR as compared to that of Pd/C (black curve). Conversely, when modifying Ag/C with Pd, the ORR $E_{1/2}$ was shifted to more positive values, toward Pd/C. In comparison to Ag/C the overpotential is significantly reduced along with an overall activity increment observed as an increase in j_D as can be observed in Figure 1a, Ag@Pd/C and Pd@Ag/C outperformed Ag/C in terms of activity. This can be seen by the higher catalytic current density measured at -0.1 V vs Hg|HgO and the potential shift toward more positive potentials with values reported in Table 1. The Pd@Ag/C sample was further modified by incorporating an additional layer of Ag via Cu UPD followed by galvanic displacement (Ag@Pd@Ag/C). As can be observed from the ORR activity presented in Figure 1b, the Ag@Pd@Ag/C was less active than Pd@Ag/C. Therefore, Pd@Ag/C was further tested and compared to Ag@Pd/C.

The plots used to obtain kinetic parameters of the ORR reaction are shown in Figure S2 as well as the Koutechy–Levich plots used to calculate the total number of electrons transferred (Figure S3).²² For Pd@Ag/C the net electron transfer was 4.0, close to what has been reported for pure Pd and also close to that for Pd/C (3.9) as obtained in these measurements.^{11,23} The mass activity at -0.1 V vs Hg|HgO normalized by a nominal amount of Pd is shown in Figure 1b for all the tested catalysts. Pd@Ag/C is almost twice as active as Pd/C based on the generated current density per Pd. Ag@Pd/C and Ag@Pd@Ag/C were found to be less active than Pd@Ag/C. Changes in the oxygen reduction kinetic parameters indicate how the introduction of small amounts of foreign metals onto the surface of a catalyst can greatly influence the catalytic activity of the system. Mass weight % for the catalysts was determined by inductively coupled plasma-atomic emission spectroscopy (ICP-AES), and the results are shown in Table S1.

The Pd@Ag/C enhanced performance is also maintained during stability experiments where the catalysts were cycled from 0.2 to -0.8 V vs Hg|HgO for 5000 potential cycles. Figure S4 shows that incorporation of Pd into the structure prolongs the usefulness of the catalysts with reductions in j_D of less than 10%. Meanwhile, Ag/C reported a decrease in overall performance activity of 40%. These results highlight the enhancement and overall performance of the catalysts due to the presence of palladium.

Cyclic voltammetry was used to probe the surface composition of the catalysts. Figure 2 presents the cyclic voltammogram (CV) for the analyzed samples along with their starting materials (i.e., Pd/C and Ag/C). The assignment of redox reactions to the respective peaks is indicated on the basis of a comparison with the data for pure Pd/C and Ag/C in Ar-saturated 0.1 M KOH. All the peaks observed for the metals prior to the electrochemical synthesis are also present on the catalyst, suggesting the presence of an alloy where the surface is composed of both metals in the resulting structure. The CV for pure Pd/C contains the respective characteristic adsorption and desorption of H_{UPD} at potentials of -0.6 to -1.0 V, along with the expected Pd oxide reduction at -0.40 V vs Hg|HgO. For the Ag/C, no distinctive adsorption and desorption of

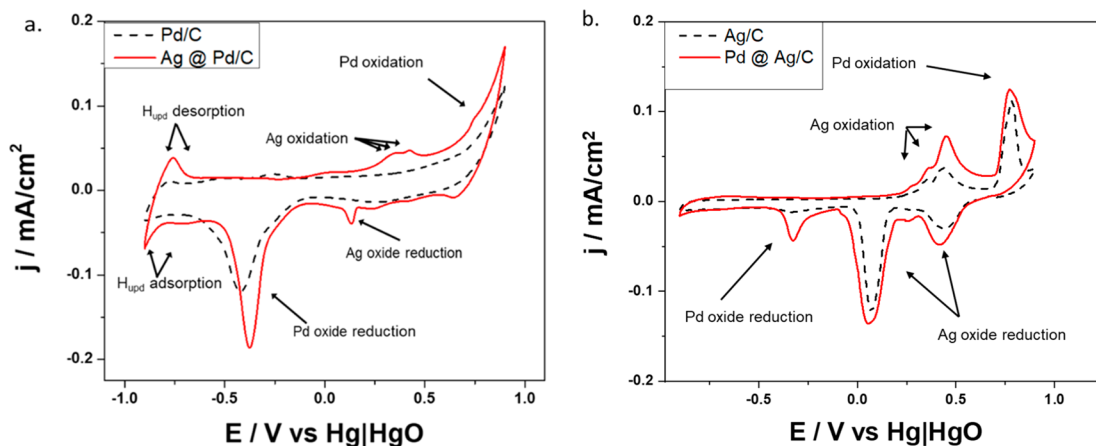


Figure 2. Cyclic voltammograms of (a) Pd/C and Ag@Pd/C, and (b) Ag/C and Pd@Ag/C measured in Ar-purged 0.1 M KOH at 50 mV/s. The CVs in part a show the characteristic peaks for Pd/C and the incorporation of Ag²⁺. The surface shows that the active surface is composed of both metals confirming the behavior of an alloy. The CVs in part b show Ag/C and the incorporation of Pd²⁺. The absence of H_{UPD} peaks suggests minimum cluster sizes of Pd dimers are at the surface.²⁷

H_{UPD} features are observed.²⁴ When the potential is scanned from 0.25 to 0.5 V vs Hg|HgO, three characteristic oxidation peaks can be observed corresponding to Ag_2O monolayer formation, AgOH bulk and Ag_2O bulk.^{25,26} In the anodic sweep, the Ag@Pd/C exhibits two characteristic peaks associated with Ag and Pd oxidation at the surface while the cathodic sweep shows the reduction of the Ag_2O and PdO, indicating that both metals are electroactive at the surface of the catalyst. The voltammogram for Pd@Ag/C also shows distinctive features corresponding to the presence of both metals at the surface. Pd@Ag/C voltammetry profiles do not show distinctive hydrogen adsorption/desorption features like those for Pd/C. This feature has been previously reported using Pd–Au alloys which hypothesized that a minimum cluster size of Pd dimers is required to exhibit adsorption/desorption behavior.²⁷ Hence, this study proposes that Pd atoms are dispersed in Ag rich surface domains, as the CV results demonstrate that both studied metals are available at the surface, regardless of the deposition arrangement.

Adding a Ag layer onto Pd@Ag/C still shows the features for Ag and Pd; however, the Ag peaks become broader while the Pd reduction peak magnitude shifts (Figure S5). Thus, the CV validates that the surface becomes Ag rich. In turn, this increased the overpotential for the ORR and was detrimental for the activity as compared to Pd@Ag/C. It further indicates that the ORR reaction is strongly dependent on the nature of the active sites present at the surface.

Details of the prepared catalyst's morphology were obtained by HR-TEM analysis on fresh samples. Figure 3a shows the

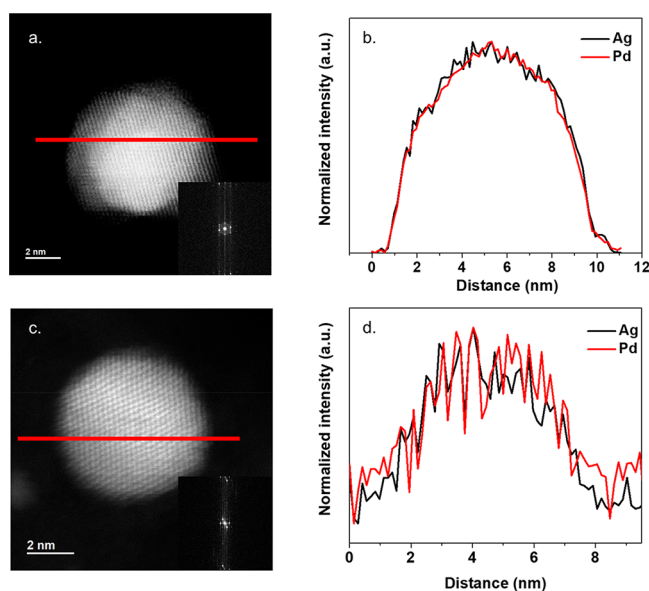


Figure 3. (a) Scanning transmission electron microscopy (STEM) and (b) electron energy loss spectroscopy (EELS) of Pd@Ag/C alloys created electrochemically and (c) STEM and (d) EELS of Ag@Pd/C alloys created electrochemically. The uniform composition of the AgPd alloy is confirmed by the EELS line scan.

image for Pd@Ag/C where small Pd species cover the Ag NP uniformly, while part b shows Ag being dispersed over Pd/C. TEM images of the starting commercial Ag/C and Pd/C materials are shown in Figure S6. The elemental composition, examined by EELS, for both alloys showed a homogeneous distribution of Pd and Ag particles, and local probing revealed an average particle size of ~ 5 nm. These results confirm the

behavior of the nanoparticle alloy consisting of both metals at the surface, as opposed to a core–shell. It has been previously reported that the composition of both metals at the surface can enhance the catalytic activity through an ensemble effect, where both metals interact in synergy at the reaction's active site promoting faster kinetics.¹¹

The increased performance for the bimetallic catalysts can be traced to a combination of factors in which ligand effects and the enrichment of metals at the surface of the catalyst seem to play a crucial role. For that matter, XAS measurements were taken at the L_{III} (Pd) and K (Pd and Ag) absorption edges. XANES at the L_{III} -edge is sensitive to the unoccupied portion of electronic density of state of d character. For Pd, the XANES data at the L_{III} -edge energy exhibits a sharp, intense peak, which is an ideal probe for studies of Pd-based catalysts since the p–d transition is particularly sensitive to changes upon alloying.²⁸

Figure S7 shows the resonance peak at the absorption Pd L_{III} -edge, also known as the white line (WL) arising from the 2p–4d transition.²⁸ The intensity of the WL decreases with d band occupancy, and this line is particularly strong for transition metals with a partially filled d band. A distinct sharp white line was observed for the reference $\text{Pd}(\text{NO}_3)_2$ and Pd/C materials. Both synthesized catalysts (Pd@Ag/C and Ag@Pd/C) exhibit an attenuation of the white line intensity, consistent with alloy formation.²⁸ Sham et al.'s studies found that, relative to the pure element, Pd gains d and loses non-d (s and p) charge upon alloying. This phenomenon can be attributed to a decrease of the number of 4d holes in Pd mainly due to a shift of electron density from the Ag to the Pd metal based on differences in their electronegativity.²⁹ Not exposing the catalyst to the Cu UPD step before galvanic displacement (PdAg/C and AgPd/C in Figure S8) resulted in no intimate interaction between Ag and Pd. Figure S8 shows a comparison of the samples of PdAg/C and AgPd/C where their white line intensity is noticeably sharper and does not resemble that of the alloys obtained and the behavior obtained for Pd L_{III} -edge when alloyed. Hence, the electrochemical synthesis steps are crucial for an intimate Pd–Ag interaction.

The analysis of atomic structure of the alloys was carried out by EXAFS using both Pd and Ag K-edges to elucidate the active structure of the catalysts within the nearest vicinity (the first coordination sphere) of each metal species. Figure 4a,b shows the XANES spectra of Pd and Ag K-edges, and Figure 4c,d shows the Fourier transform magnitudes of the EXAFS data spectra of Pd and Ag K-edges presented in Figure S9. The Pd K-edge white line intensity for the alloy samples resembles that of Pd foil. On the other hand, the Pd/C sample has a sharper white line suggesting a higher oxidation state than pure Pd. For Ag@Pd/C, the electrochemical treatment modifies the Pd/C electronic structure and reduces Pd at the bulk with an electronic transfer from Ag to Pd. This coincides with the Fourier transform where the Pd foil magnitude is similar to those of the alloy. The Ag K-edge shows more remarkable differences for the alloyed samples as compared to the Ag foil presumably due to net electron transfers from Ag to Pd. The data strongly suggests a significant change in coordination for both elements as they interact with each other. For that matter, the results of EXAFS fitting as well as the fitting performed for each of the prepared catalyst at each respective metal's absorption edge are summarized in Table 2. Since Pd and Ag are adjacent in the periodic table, their photoelectron scattering amplitudes and phase shifts are similar; the method

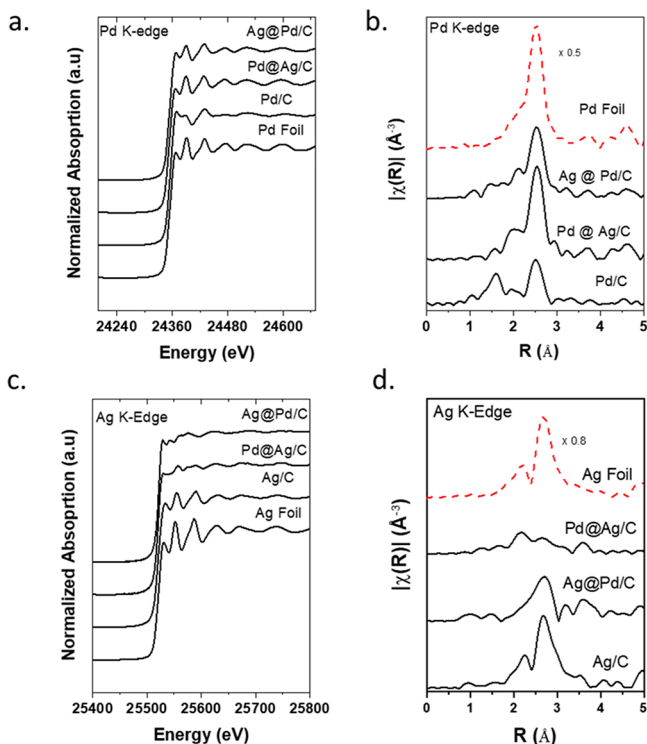


Figure 4. (a) XANES data at the Pd K-edge and corresponding (b) Fourier transform magnitude. (c) XANES data at the Ag K absorption edge and (d) corresponding Fourier transform magnitude of the synthesized samples with corresponding reference.

could not, in principle, discriminate between Pd–Pd and Pd–Ag bonds for Pd absorbers (or Ag–Ag and Ag–Pd for Ag absorbers). The subtle differences between neighboring species around the central atom make it difficult to conclude whether an alloy is formed. However, their lattice parameters are significantly different, and Ag has a larger atomic radius than Pd therefore, the interaction between both metals changes the bond length compared to their respective starting materials (Ag/C and Pd/C). From these results, it can be observed that the Pd–Pd coordination number (CN) for the foil is 12 with a bond length of 2.737 Å. However, the Pd/C nanoparticles used for the synthesis have a shorter bond length, consistent with the smaller size of Pd nanoparticles as compared to the Pd foil bulk. Pd/C also exhibits a peak around 2.0 Å related to the Pd–O bond length as has been previously reported.³⁰ When Ag is incorporated into the structure (Ag@Pd/C), the bond length of Pd–Pd(Ag) increases to 2.747 Å, which is longer than the initial Pd foil or the Pd/C radial distance and originates

from the interaction of Pd with the Ag atom. From the Ag K-edge perspective, it can be observed that there is a decrease in the bond length for Ag@Pd/C (from 2.860 to 2.786 Å).

On the other hand, for Pd@Ag/C, the Pd and the Ag absorption edges show a similar trend in terms of the radial distance, obtained where the bond length of Pd increases and the bond length of Ag decreases. However, from the Pd edge perspective, the Pd–Pd CN value increased while, from the Ag K-edge, the Ag–Ag(Pd) CN decreased to 1.7. This small CN is attributed to small interactions between Ag and Cl from the PdCl₂ precursor. For that matter, the synthesis was carried out using Pd(NO₃)₂ as a precursor to substitute PdCl₂. Thereafter, the catalyst was evaluated for ORR activity (Figure S10) at 1600 rpm, showing less catalytic improvement as compared to when PdCl₂ was used as precursor and was not used for further experiments.

XANES and EXAFS analyses confirms the strong interaction between Pd and Ag metals obtained using the electrochemical synthesis. There is a net electron transfer from Ag to Pd based on the reduced white line intensity observed in the XANES as well as the expansion of Pd and contraction of Ag radius for both alloys. However, electrochemical reactions are significantly more sensitive to the surface of the catalyst exposed to the solution. For that matter, XPS is significantly more sensitive to the surface composition rather than the bulk material; thus, it was used to examine the chemical and electronic composition of Pd and Ag of these catalysts.

Pd/C spectra show a characteristic electronic transition (3d_{5/2}) with a doublet located at 335.1 eV.³¹ As demonstrated in Figure 5a, the Pd 3d spectrum for Pd/C with binding energy

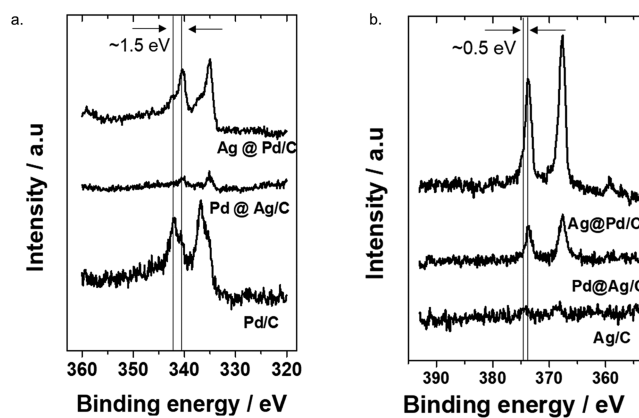


Figure 5. X-ray photoelectron spectroscopy spectra for (a) Pd 3d and (b) Ag 3d binding energy regions for both Pd:Ag alloys and the commercial catalysts Ag/C and Pd/C.

Table 2. Fit Parameters of the Catalysts Determined by the EXAFS Fitting

sample name	K-edge	near neighbor species	N	R (Å)	σ^2 (Å ²)	E_0 (eV)
Ag foil	Ag	Ag	12	2.860 ± 0.002	0.0095 ± 0.0003	0.6 ± 0.3
Ag/C	Ag	Ag	10.7 ± 0.6	2.861 ± 0.003	0.0095 ± 0.0005	0.8 ± 0.4
Ag@Pd/C	Ag	Pd/Ag	9.3 ± 0.6	2.786 ± 0.004	0.0096 ± 0.0006	0.1 ± 0.5
Pd@Ag/C	Ag	Cl	1.7 ± 0.6	2.72 ± 0.03	0.001 ± 0.005	5.6 ± 2.7
Pd foil	Pd	Pd	12	2.737 ± 0.002	0.0056 ± 0.0002	−1.5 ± 0.4
Pd/C	Pd	O	3.5 ± 1.1	2.06 ± 0.01	0.003 ± 0.003	2.7 ± 1.2
		Pd	5.5 ± 1.0	2.732 ± 0.007	0.007 ± 0.001	2.7 ± 1.2
Ag@Pd/C	Pd	O	1.4 ± 0.6	2.06 ± 0.02	0.005 ± 0.005	2.2 ± 0.4
		Pd/Ag	8.7 ± 0.5	2.747 ± 0.002	0.0063 ± 0.0003	2.2 ± 0.4
Pd@Ag/C	Pd	Pd/Ag	10.3	2.746 ± 0.003	0.0065 ± 0.0004	−2.6 ± 0.5

of 336.7 and 342.0 eV indicated that Pd was predominantly present in its oxidized state. Once the Ag is incorporated into the structure (Ag@Pd/C), the binding energy shifts to 335.1 and 340.3 eV, consistent with the observations from PdAg alloy formation at the surface. While Pd was expected to be enriched at the surface of Pd@Ag/C based on the electrochemical technique used for deposition, the Pd 3d peak had a lower intensity compared to that of Ag@Pd/C. This supports the hypothesis of preferential enrichment of Ag at the surface based on differences in their surface energy.

Figure 5b exhibits the $3d_{5/2}$ transition for Ag with a doublet located at 368.3 eV.³¹ The initial Ag/C 3d binding energy peak is barely visible; this is attributed to Ag being buried within the carbon which attenuates the photoelectron traveling through an attenuating medium. Nonetheless, the Ag peak intensity increases when Pd is incorporated via galvanic displacement. This is an indication that the incorporation of Pd not only perturbed the electronic structure of Ag, but also exposed Ag to the surface. Ag@Pd/C showed the sharpest peak mainly due to the segregation effects from the enrichment of Ag at the surface. This behavior has been previously reported on a Pd–Ag film, where Pd gains electron density from Ag, shifting the binding energy of Ag due to a gain of charge density in the d band, with a concomitant loss in the sp band.^{28,32} Consequently, Ag is enriching the surface to a higher extent in Ag@Pd/C than in Pd@Ag/C. By this interaction, the incorporation of Pd into Ag/C weakens the intensity of the $3d_{5/2}$ transition signal compared to Ag incorporated into Pd/C.

The electronic shift according to XPS shows a synergy in activity between the alloy ratio relative to its pure components particularly for the Pd@Ag/C catalyst with minimal loading. This synergy is favored by the high degree Pd–Ag contacts versus Pd–Pd contacts, which modified the Pd electronic structure as evaluated by XPS and XAS. The electronic structure of Ag is similar to Au with a filled d shell, which explains why Ag lies on the weak binding site of the volcano plot for activity by d band charge theory. For that matter, Ag is expected to show weak oxygen binding resulting in low binding affinity toward the first electron transfer step. Increasing the d band charge density by incorporating Pd facilitates the initial electron transfer which contributes to strong oxygen binding via ensemble effects where two different metal atoms catalyze distinct steps in the reaction mechanism.³³ This approach of combining metals with a resulting higher activity is based on simple thermodynamic principles assuming a simple mechanism where one metal breaks the oxygen bond of molecular O_2 and the other metal reduced the resulting chemisorbed atomic oxygen.³³

Higher reactivity for the Pd@Ag/C can be explained by the different metal compositions at the surfaces of the catalysts compared to their compositions at the bulk. XAS data helped to elucidate the electronic distribution of the materials where they share a similar structure. There is a net transfer from the less electronegative Ag atom to Pd, ultimately reducing the white line intensity and resembling the Pd foil. On the other hand, the Ag spectra for the alloys exhibit a sharp white line in agreement with data for oxidized Ag for both alloys. However, these results do not account for the higher reactivity of one metal alloy over the other. As previously mentioned, the surface of the catalyst is strongly influenced by the segregation of metals to the surface. Although the bulk of the material may be composed of a specific ratio, the Ag alloy components enrich the surface region, which is sensitive to electrochemical

techniques. Nørksov et al. studied the chemical composition at the surface of an alloy and concluded that it may differ from the composition in the bulk.³⁴ It has been well-noted that the surface composition of most alloys is particularly sensitive to the external conditions, including the methodology used for deposition. Although this hypothesis has been applied to numerous systems, the behavior obtained does not necessarily predict the correct segregation under experimental conditions.

An XPS peak fitting for the elemental composition at the surface is shown in Figure S11. To obtain a comparable relative concentration, the areas were adjusted by the atomic sensitivity factor. For Pd@Ag/C, the atomic contribution at the surface was calculated and a 1:2 ratio for Pd to Ag was found whereas for Ag@Pd/C the atomic ratio was found to be 1:1. For solids, surface segregation can be translated to the mixing of heat, surface energy difference, and relative atomic size. Experimentally the surface energy has been calculated to be 1.05–1.38 J/m² for Pd and 1.38–2.17 J/m² for Ag, with ranges varying on the basis of exposed facets at the surface. As a result, the surface energy of Ag is considerably higher than that of Pd while the lattice constant of the bulk (4.09 Å) is larger than that of bulk Pd (3.88 Å).³⁵ Ag is most likely to be found at the surface since less strain results in less surface energy compared to those in the subsurface and core region which leave Ag more exposed.³⁶ Therefore, regardless of whether Ag is deposited onto Pd/C or Pd onto Ag/C, the surface becomes more Ag enriched. Interestingly, the compositional ratio at the surface for the Pd@Ag/C has an outstanding activity for ORR, compared to that of the Ag@Pd/C or Pd/C. An additional layer of Ag modifies the compositional ratio at the surface and results in a decrease in performance in activity. Having Ag and Pd at the surface deposited by electrochemical methods increased the intimate mixing between both metals which led to an increase in both electronic and ensemble effects.

CONCLUSION

The design of bimetallic alloys with atomically precise noble metal loading is of great interest in the field of catalysis. Herein, we demonstrated an electrochemical method that is able to reduce a Ag^+ or Pd^{2+} precursor onto Pd/C and Ag/C, respectively, to form alloy nanoparticles with high activities for the oxygen reduction reaction (ORR) in alkaline media. The ORR mass activities relative to pure Pd were determined at -0.1 V vs Hg/HgO showing mass activities of 321 mA/mg_{Pd} for Pd, 820 mA/mg_{Pd} for Pd@Ag/C, 366 mA/mg_{Pd} for Ag@Pd/C, and 526 mA/mg_{Pd} Ag@Pd@Ag/C. For the most active catalyst, the activity was increased 2-fold on a Pd mass basis by incorporating Pd onto Ag/C. Scanning transmission electron microscopy and electron energy loss spectroscopy probed the uniformity of the nanoparticle's local structure with no significant differences in terms of dispersion and size for each alloy. The improvement in electrocatalytic response was explained by a combination of factors involving ligand and geometric effects shown by XPS and ex situ EXAFS analysis, respectively. The segregation of Ag on a rich Ag surface 2:1 for Pd@Ag/C greatly enhanced the ORR reaction kinetics and the number of electrons transferred with respect to a 1:1 Ag to Pd ratio on the Ag@Pd/C alloy and pure Pd. Moreover, the enhancement in catalytic activity was associated with the presence of both Ag and Pd at the surface, where the steps of oxygen bond breaking and desorption for the ORR occur in synergy: the initial O_2 adsorbs at the Pd atoms followed by the rapid disproportionation step on the Ag rich surface.

■ ASSOCIATED CONTENT

Supporting Information

The Supporting Information is available free of charge at <https://pubs.acs.org/doi/10.1021/acsaem.9b01920>.

Table with details of ICP-AES analysis of catalyst materials and figures showing the synthesis of Pd/Ag/C catalysts by galvanic displacement of UPD Cu, ORR RDE thermodynamic parameters of catalysts, catalyst ORR RDE measurements, stability ORR polarization curves of catalysts, cyclic voltammetry of catalysts, TEM and particle size histogram of catalysts, Pd L₃-edge XANES of alloys with and without the Cu UPD treatment relative to Pd/C and Pd@Ag/C, XAFS data in *k* space for Pd and Ag K-edges for all catalysts, ORR RDE measurements, and X-ray photoelectron spectroscopy of Ag 3d and Pd 3d binding energy curve fitting (PDF)

■ AUTHOR INFORMATION

Corresponding Author

Carlos R. Cabrera – Department of Chemistry, University of Puerto Rico—Rio Piedras Campus, San Juan, Puerto Rico 00925-2537, United States; orcid.org/0000-0002-3342-8666; Email: carlos.cabrera2@upr.edu

Authors

Luis E. Betancourt – Chemistry Division, Brookhaven National Laboratory, Upton, New York 11973, United States

Arnulfo Rojas-Pérez – Department of Chemistry, University of Puerto Rico—Rio Piedras Campus, San Juan, Puerto Rico 00925-2537, United States; orcid.org/0000-0002-3804-6309

Ivan Orozco – Chemistry Division, Brookhaven National Laboratory, Upton, New York 11973, United States

Anatoly I. Frenkel – Chemistry Division, Brookhaven National Laboratory, Upton, New York 11973, United States; Department of Materials Science and Chemical Engineering, Stony Brook University, New York, New York 11794, United States; orcid.org/0000-0002-5451-1207

Yuanyuan Li – Department of Materials Science and Chemical Engineering, Stony Brook University, New York, New York 11794, United States

Kotaro Sasaki – Chemistry Division, Brookhaven National Laboratory, Upton, New York 11973, United States; orcid.org/0000-0003-2474-8323

Sanjaya D. Senanayake – Chemistry Division, Brookhaven National Laboratory, Upton, New York 11973, United States; orcid.org/0000-0003-3991-4232

Complete contact information is available at: <https://pubs.acs.org/doi/10.1021/acsaem.9b01920>

Notes

The authors declare no competing financial interest.

■ ACKNOWLEDGMENTS

This work was financially supported by the NSF-CREST Center for Innovation, Research and Education in Environmental Nanotechnology Grant HRD-1736093 and NSF-PREM Center for Interfacial Electrochemistry of Energy Materials Grant DMR-1827622. EXAFS analysis and modeling of Ag–Pd interactions by AIF were supported as part of the Integrated Mesoscale Architectures for Sustainable Catalysis

(IMASC), an Energy Frontier Research Center funded by the U.S. Department of Energy, Office of Science, Basic Energy Sciences under Award DE-SC0012573. This research used resources of the Center for Functional Nanomaterials (CFN), which is a U.S. DOE Office of Science Facility, at Brookhaven National Laboratory (BNL) under Contract DE-SC0012704. We thank Kim Kisslinger (CFN-BNL) for assistance with the TEM images. This research used resources of beamline 8-ID and 8-BM of the National Synchrotron Light Source II, a U.S. Department of Energy (DOE) Office of Science User Facility operated for the DOE Office of Science by Brookhaven National Laboratory under Contract DE-SC0012704.

■ REFERENCES

- (1) Shao, M.; Chang, Q.; Dodelet, J.-P.; Chenitz, R. Recent Advances in Electrocatalysts for Oxygen Reduction Reaction. *Chem. Rev.* **2016**, *116* (6), 3594–3657.
- (2) Xiong, Y.; Yang, Y.; Feng, X.; DiSalvo, F. J.; Abruña, H. D. A Strategy for Increasing the Efficiency of the Oxygen Reduction Reaction in Mn-Doped Cobalt Ferrites. *J. Am. Chem. Soc.* **2019**, *141* (10), 4412–4421.
- (3) Zhong, H.; Luo, Y.; He, S.; Tang, P.; Li, D.; Alonso-Vante, N.; Feng, Y. Electrocatalytic Cobalt Nanoparticles Interacting with Nitrogen-Doped Carbon Nanotube in Situ Generated from a Metal-Organic Framework for the Oxygen Reduction Reaction. *ACS Appl. Mater. Interfaces* **2017**, *9* (3), 2541–2549.
- (4) Chen, G.; Kuttiyiel, K. A.; Su, D.; Li, M.; Wang, C.-H.; Buceta, D.; Du, C.; Gao, Y.; Yin, G.; Sasaki, K.; Vukmirovic, M. B.; Adzic, R. R. Oxygen Reduction Kinetics on Pt Monolayer Shell Highly Affected by the Structure of Bimetallic AuNi Cores. *Chem. Mater.* **2016**, *28* (15), 5274–5281.
- (5) Sasaki, K.; Naohara, H.; Cai, Y.; Choi, Y. M.; Liu, P.; Vukmirovic, M. B.; Wang, J. X.; Adzic, R. R. Core-Protected Platinum Monolayer Shell High-Stability Electrocatalysts for Fuel-Cell Cathodes. *Angew. Chem., Int. Ed.* **2010**, *49* (46), 8602–8607.
- (6) Sasaki, K.; Marinkovic, N.; Isaacs, H. S.; Adzic, R. R. Synchrotron-Based In Situ Characterization of Carbon-Supported Platinum and Platinum Monolayer Electrocatalysts. *ACS Catal.* **2016**, *6* (1), 69–76.
- (7) Zhang, J.; Lima, F. H. B.; Shao, M. H.; Sasaki, K.; Wang, J. X.; Hanson, J.; Adzic, R. R. Platinum Monolayer on Nonnoble Metal-Noble Metal Core-Shell Nanoparticle Electrocatalysts for O₂ Reduction. *J. Phys. Chem. B* **2005**, *109* (48), 22701–22704.
- (8) Antolini, E. Formation of carbon-supported PtM alloys for low temperature fuel cells: a review. *Mater. Chem. Phys.* **2003**, *78* (3), 563–573.
- (9) Safavi, A.; Maleki, N.; Farjami, E. Electrodeposited Silver Nanoparticles on Carbon Ionic Liquid Electrode for Electrocatalytic Sensing of Hydrogen Peroxide. *Electroanalysis* **2009**, *21* (13), 1533–1538.
- (10) Sekol, R. C.; Li, X.; Cohen, P.; Doubek, G.; Carmo, M.; Taylor, A. D. Silver palladium core-shell electrocatalyst supported on MWNTs for ORR in alkaline media. *Appl. Catal., B* **2013**, *138–139*, 285–293.
- (11) Slanac, D. A.; Hardin, W. G.; Johnston, K. P.; Stevenson, K. J. Atomic Ensemble and Electronic Effects in Ag-Rich AgPd Nanoalloy Catalysts for Oxygen Reduction in Alkaline Media. *J. Am. Chem. Soc.* **2012**, *134* (23), 9812–9819.
- (12) Nørskov, J. K.; Rossmeisl, J.; Logadottir, A.; Lindqvist, L.; Kitchin, J. R.; Bligaard, T.; Jónsson, H. Origin of the Overpotential for Oxygen Reduction at a Fuel-Cell Cathode. *J. Phys. Chem. B* **2004**, *108* (46), 17886–17892.
- (13) Roy, A.; Pal, T. Silver-induced electronic drift in AgPd bimetals: rationale for enhanced electrocatalytic activity of ethanol oxidation reaction. *New J. Chem.* **2017**, *41* (20), 12278–12287.
- (14) Stamenkovic, V.; Mun, B. S.; Mayrhofer, K. J. J.; Ross, P. N.; Markovic, N. M.; Rossmeisl, J.; Greeley, J.; Nørskov, J. K. Changing the Activity of Electrocatalysts for Oxygen Reduction by Tuning the

Surface Electronic Structure. *Angew. Chem., Int. Ed.* **2006**, *45* (18), 2897–2901.

(15) Erikson, H.; Sarapuu, A.; Solla-Gullón, J.; Tammeveski, K. Recent progress in oxygen reduction electrocatalysis on Pd-based catalysts. *J. Electroanal. Chem.* **2016**, *780*, 327–336.

(16) Zhang, L.; Chang, Q.; Chen, H.; Shao, M. Recent advances in palladium-based electrocatalysts for fuel cell reactions and hydrogen evolution reaction. *Nano Energy* **2016**, *29*, 198–219.

(17) Erikson, H.; Sarapuu, A.; Tammeveski, K. Oxygen Reduction Reaction on Silver Catalysts in Alkaline Media: a Minireview. *ChemElectroChem* **2019**, *6* (1), 73–86.

(18) Yamamoto, M.; Kakiuchi, H.; Kashiwagi, Y.; Yoshida, Y.; Ohno, T.; Nakamoto, M. Synthesis of Ag-Pd Alloy Nanoparticles Suitable as Precursors for Ionic Migration-Resistant Conductive Film. *Bull. Chem. Soc. Jpn.* **2010**, *83* (11), 1386–1391.

(19) Lüsi, M.; Erikson, H.; Merisalu, M.; Kasikov, A.; Matisen, L.; Sammelselg, V.; Tammeveski, K. Oxygen Electroreduction in Alkaline Solution on Pd Coatings Prepared by Galvanic Exchange of Copper. *Electrocatalysis* **2018**, *9* (3), 400–408.

(20) Ravel, B.; Newville, M. ATHENA, ARTEMIS, HEPHAESTUS: data analysis for X-ray absorption spectroscopy using IFEFFIT. *J. Synchrotron Radiat.* **2005**, *12* (4), 537–541.

(21) Blyth, R. I. R.; Buqa, H.; Netzer, F. P.; Ramsey, M. G.; Besenhard, J. O.; Golob, P.; Winter, M. XPS studies of graphite electrode materials for lithium ion batteries. *Appl. Surf. Sci.* **2000**, *167* (1–2), 99–106.

(22) Bard, A. J.; Faulkner, L. R. *Electrochemical Methods: Fundamentals and Applications*; Wiley & Sons: New York, 2002.

(23) Wang, M.; Qin, X.; Jiang, K.; Dong, Y.; Shao, M.; Cai, W.-B. Electrocatalytic Activities of Oxygen Reduction Reaction on Pd/C and Pd-B/C Catalysts. *J. Phys. Chem. C* **2017**, *121* (6), 3416–3423.

(24) Spendelov, J. S.; Wieckowski, A. Electrocatalysis of oxygen reduction and small alcohol oxidation in alkaline media. *Phys. Chem. Chem. Phys.* **2007**, *9* (21), 2654–2675.

(25) Guo, J.; Hsu, A.; Chu, D.; Chen, R. Improving Oxygen Reduction Reaction Activities on Carbon-Supported Ag Nanoparticles in Alkaline Solutions. *J. Phys. Chem. C* **2010**, *114* (10), 4324–4330.

(26) Hepel, M.; Tomkiewicz, M. Study of the Initial Stages of Anodic Oxidation of Polycrystalline Silver in KOH Solutions. *J. Electrochem. Soc.* **1984**, *131* (6), 1288–1294.

(27) Maroun, F.; Ozanam, F.; Magnussen, O. M.; Behm, R. J. The Role of Atomic Ensembles in the Reactivity of Bimetallic Electrocatalysts. *Science* **2001**, *293* (5536), 1811.

(28) Coulthard, I.; Sham, T. K. Charge Redistribution in Pd-Ag Alloys from a Local Perspective. *Phys. Rev. Lett.* **1996**, *77* (23), 4824–4827.

(29) Witjens, L. C.; Bitter, J. H.; van Dillen, A. J.; de Jong, K. P.; de Groot, F. M. F. Pd L3 edge XANES investigation of the electronic and geometric structure of Pd/Ag-H membranes. *Phys. Chem. Chem. Phys.* **2004**, *6*, 3903–3906.

(30) Sasaki, K.; Naohara, H.; Choi, Y.; Cai, Y.; Chen, W.-F.; Liu, P.; Adzic, R. R. Highly stable Pt monolayer on PdAu nanoparticle electrocatalysts for the oxygen reduction reaction. *Nat. Commun.* **2012**, *3*, 1115.

(31) Mouder, J. F.; Stickle, W. F.; Sobol, P. E.; Bomben, K. D. *Handbook of X-Ray Photoelectron Spectroscopy*; Perkin-Elmer-Corp: Eden Prairie, MN, 1992.

(32) Sham, T. K.; Naftel, S. J.; Coulthard, I. M_{3,2}-edge x-ray absorption near-edge structure spectroscopy: An alternative probe to the L_{3,2}-edge near-edge structure for the unoccupied densities of d states of 5d metals. *J. Appl. Phys.* **1996**, *79* (9), 7134–7138.

(33) Fernández, J. L.; Walsh, D. A.; Bard, A. J. Thermodynamic Guidelines for the Design of Bimetallic Catalysts for Oxygen Electroreduction and Rapid Screening by Scanning Electrochemical Microscopy. M-Co (M: Pd, Ag, Au). *J. Am. Chem. Soc.* **2005**, *127* (1), 357–365.

(34) Liu, P.; Norskov, J. K. Ligand and ensemble effects in adsorption on alloy surfaces. *Phys. Chem. Chem. Phys.* **2001**, *3* (17), 3814–3818.

(35) Sinnott, S. B.; Stave, M. S.; Raeker, T. J.; DePristo, A. E. Corrected effective-medium study of metal-surface relaxation. *Phys. Rev. B: Condens. Matter Mater. Phys.* **1991**, *44* (16), 8927–8941.

(36) Kuijers, F. J.; Ponc, V. The surface composition of PdAg alloys. *J. Catal.* **1979**, *60*, 100–109.